PHILOSOPHICAL TRANSACTIONS OF THE ROYAL SOCIETY A MATHEMATICAL, PHYSICAL & ENGINEERING SCIENCES

Multiphoton absorption by multielectron atoms

K.T. Taylor and D. Dundas

Phil. Trans. R. Soc. Lond. A 1999 **357**, 1331-1358
doi: 10.1098/rsta.1999.0377

THE ROYAL SOCIETY

Multiphoton absorption by multielectron atoms

By K. T. Taylor and D. Dundas†

Department of Applied Mathematics and Theoretical Physics, The Queen's University of Belfast, Belfast BT7 1NN, UK

A survey is presented of time-independent and time-dependent methods that have been developed over the past decade to investigate the interactions between multielectron atoms and very intense laser radiation. Sample results are presented.

Keywords: intense laser radiation; laser-driven atoms; high-harmonic generation; above-threshold ionization; computational methods; scientific visualization analysis

1. Introduction

Over the past decade, the theoretical interest in multiphoton absorption by atoms has moved more and more away from single-electron atoms to those with few or many electrons. Several matters have either stimulated or mediated this shift of interest. From the physics point of view, curiosity about the role of the electron–electron interaction has been a strong motivator. From the practical point of view, the steadily increasing power of workstations and supercomputers over the decade has made worthwhile calculations possible.

In this article, we briefly survey those methods, beyond the level of perturbation theory, that have been developed to investigate the response of multielectron atoms to very intense laser radiation. The methods fall naturally into two classes: time-independent and time-dependent, and can be thought of as appropriate for handling laser pulses longer and shorter, respectively, than about 1 ps. In §§ 2 and 3 these classes are handled in turn. Finally, some conclusions are drawn in § 4.

2. Time-independent methods

Two distinct methods of this type have been developed based, respectively, on R-matrix Floquet theory and on many body S-matrix theory. The former has been developed with a general multielectron atom in mind, and yields information on many laser-induced and laser-assisted processes, while the latter, at present, specifically addresses double ionization in helium.

(*a*) *R-matrix Floquet theory*

Assuming that the laser field is spatially homogeneous, harmonic and monochromatic and can be treated classically, the semi-classical Hamiltonian for the system can be written as

$$H(t) = H_{\mathrm{a}} + H_{\mathrm{i}}(t), \tag{2.1}$$

† Present address: Department of Physics, University of Durham, Durham DH1 3LE, UK.

where H_a is the field-free atomic Hamiltonian and $H_i(t)$ represents the time-dependent interaction between the field and the atom, which is periodic. The interaction term can be decomposed into two parts

$$H_i(t) = V_+ e^{i\omega t} + V_- e^{-i\omega t}, \tag{2.2}$$

which correspond to absorption or emission of a photon, and where $V_- = V_+^\dagger$. The Floquet ansatz allows the state vector of the system to be written as (Floquet 1883)

$$|\Psi(t)\rangle = e^{-iEt}|\psi(t)\rangle, \tag{2.3}$$

where $\psi(t)$ is the time-periodic Floquet vector and E is the complex time-independent pseudo-energy

$$E = E_0 + \Delta - \tfrac{1}{2}i\Gamma, \tag{2.4}$$

E_0 being the unperturbed field-free energy of the initial state, Δ the AC Stark shift, and Γ the width of the state that represents the total ionization rate.

The Floquet vector can be expanded as a Fourier series

$$|\psi(t)\rangle = \sum_n e^{-in\omega t}|\psi_n\rangle, \tag{2.5}$$

with each $|\psi_n\rangle$ corresponding to the absorption or emission of n photons. Substituting this expansion in the time-dependent Schrödinger equation (TDSE) yields an infinite set of coupled time-independent equations (Potvliege & Shakeshaft 1988)

$$(H_a - E - N\omega)|\psi_n\rangle = V_+|\psi_{n-1}\rangle + V_-|\psi_{n+1}\rangle, \tag{2.6}$$

for the harmonic components. The coupled equations defined by equation (2.6) can be written as the eigenvalue equation

$$(\boldsymbol{H}_F - E)|\boldsymbol{\psi}^L\rangle = 0, \tag{2.7}$$

where the Floquet–Hamiltonian ($\boldsymbol{H}_F$) is an infinite block-tridiagonal matrix of operators with a repetitive structure given by

$$\boldsymbol{H}_F = \begin{bmatrix} \ddots & & & & & \\ & V & & & & \\ & H_a - (n-1)\omega & V & & & \\ & V^\dagger & H_a - n\omega & V & & \\ & V^\dagger & H_a - (n+1)\omega & & & \\ & & & V^\dagger & & \\ & & & & \ddots & \end{bmatrix}. \tag{2.8}$$

In practical calculations this infinite matrix is truncated at the smallest number of blocks required to obtain convergence for the multiphoton process under study.

We now discuss how the Floquet method has been extended to treat complex atoms and ions by combining it with the R-matrix method developed by Wigner (1946) to study nuclear collisions, and adapted by Burke *et al.* (1971) to study atomic and molecular scattering processes. This theory, which expands the harmonic components in equation (2.5) on the R-matrix basis as proposed by Burke *et al.* (1990, 1991) and extended by Dörr *et al.* (1992), has become known as the R-matrix Floquet (RMF) method.

(i) *The basic equations*

Consider an atomic system with $N+1$ electrons (N residual electrons and one ejected electron) in a laser field. Working in the dipole approximation, the minimal coupling form of the TDSE for such a system is given by

$$\mathrm{i}\frac{\partial}{\partial t}\Psi(\boldsymbol{X}_{N+1},t)=\left[H_{N+1}+\frac{1}{c}\boldsymbol{A}(t)\cdot\boldsymbol{P}_{N+1}\right]\Psi(\boldsymbol{X}_{N+1},t), \tag{2.9}$$

where $\boldsymbol{X}_{N+1}\equiv(\boldsymbol{x}_1,\ldots,\boldsymbol{x}_{N+1})$, and where $\boldsymbol{x}_i\equiv(\boldsymbol{r}_i,\boldsymbol{\sigma}_i)$ are, respectively, the space and spin coordinates of the ith electron, H_{N+1} is the field-free Hamiltonian of the $(N+1)$-electron atomic system, $\boldsymbol{P}_{N+1}$ is the total momentum operator and $\boldsymbol{A}(t)$ is the vector potential describing the laser field. As in field-free R-matrix theory, configuration space is divided into an inner region and an outer region. All the electrons can be found in the inner region (extending to a radius a), while only one electron is permitted in the outer region. Thus, an immediate drawback of the method as so far implemented is its limitation to model only single-electron ionization. It is found that a length-gauge description in the inner region leads to very fast convergence properties of the R-matrix. Using this gauge, the laser–atom coupling also tends to zero at the origin. In the outer region, although the matrix elements remain accurate, a length-gauge description would result in the $\boldsymbol{E}\cdot\boldsymbol{r}$ coupling term exploding as the radial distance, r, increases. Therefore, a velocity-gauge description is used to describe the interaction between the field and the electron in the outer region. A gauge transformation is performed on the boundary between the regions.

(ii) *The inner-region solution*

Equation (2.7) is the starting point but the Hamiltonian is not Hermitian in this finite region. This can be remedied by introducing a Bloch operator (Bloch 1957), $\boldsymbol{L}_{\mathrm{B}}$, on the surface of this region at $r=a$ so that $\boldsymbol{H}_{\mathrm{F}}+\boldsymbol{L}_{\mathrm{B}}$ is Hermitian. An R-matrix basis (Burke *et al*. 1971) is then employed, namely

$$\psi_{kn}(\boldsymbol{X}_{N+1})=\mathcal{A}\sum_{\Gamma i\ell}\varphi_i^{\Gamma}(r_j^{-1})r_j^{-1}u_\ell^{\Gamma}(r_j)a_{i\ell kn}^{\Gamma}+\sum_{\Gamma i}\mathcal{X}_i^{\Gamma}(\boldsymbol{X}_{N+1})b_{ikn}^{\Gamma}, \tag{2.10}$$

where $\mathcal{A}$ is the Pauli antisymmetrization operator, u_ℓ^{Γ} are radial basis functions that are non-vanishing on the surface, $\mathcal{X}_i^{\Gamma}$ are quadratically integrable antisymmetric functions that vanish by the surface of the internal region, $a_{i\ell kn}^{\Gamma}$ and b_{ikn}^{Γ} are found by diagonalizing $\boldsymbol{H}_{\mathrm{F}}+\boldsymbol{L}_{\mathrm{B}}$, and the $\varphi_i^{\Gamma}(r_j^{-1})$ are formed by coupling the atomic target states with the spin-angle functions of the scattered or ejected electron (j), to give a state whose quantum numbers are collectively denoted by Γ (not to be confused with the width of the pseudo-energy defined by equation (2.4)).

The spectral representation of the operator $\boldsymbol{H}_{\mathrm{F}}+\boldsymbol{L}_{\mathrm{B}}$ is used to obtain the relation

$$\boldsymbol{F}(a)=\boldsymbol{R}(E)\left[r\frac{\mathrm{d}\boldsymbol{F}}{\mathrm{d}r}\right]_{r=a}, \tag{2.11}$$

where $\boldsymbol{R}$ is the R-matrix, and $\boldsymbol{F}(r)$ denotes the reduced radial functions. The R-matrix will be inaccurate due to truncation in the number of continuum orbitals retained, and so convergence is improved by the addition of a Buttle correction to the diagonal elements (Buttle 1967).

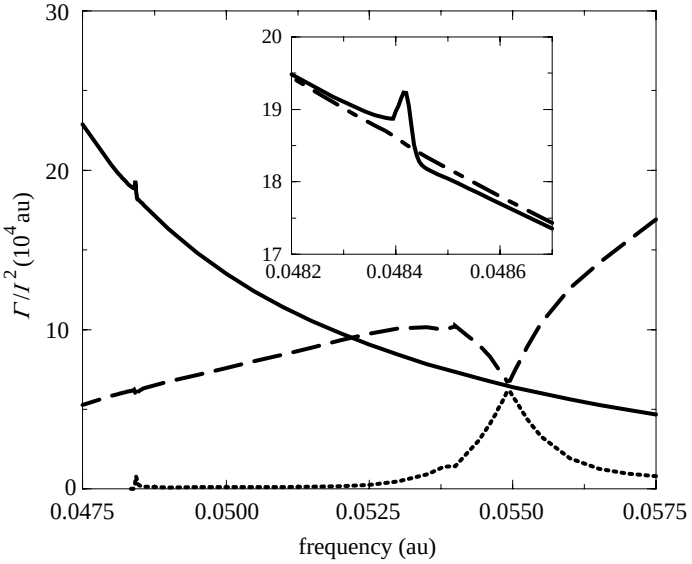

Figure 1. Partial multiphoton detachment rates for the multiphoton detachment of Li^-. The two-photon rates leaving the residual atom in the 2s (full) and 2p (dashed) states, and the three-photon rate leaving the atom in the 3s state (dotted) divided by the intensity squared are shown for an intensity of 1.0×10^{10} W cm^{-2}. The inset also gives the partial rate leaving the atom in the 2s state for an intensity of 1.0×10^9 W cm^{-2} (chain).

Equation (2.11) is the basic equation that describes the solution of the TDSE in the inner region, demonstrating the connection between the logarithmic derivative of the wave function for the ejected electron on the boundary, $r = a$, and the R-matrix. This provides the initial conditions for solving equation (2.9) in the outer region.

(iii) *The outer-region solution*

The outer-region electron is treated in the velocity gauge. As in the inner region, the Fourier–Floquet expansion is invoked, which results in harmonic equations taking the same form as equation (2.6). However, instead of the R-matrix basis functions used for the inner-region solution, a close-coupling expansion is employed:

$$\psi_n^V(\boldsymbol{X}_{N+1}) = \sum_{\Gamma_i} \varphi_i^\Gamma(r_{N+1}^{-1}) r_{N+1}^{-1} {}^V G_{in}^\Gamma r_{N+1}^{-1} {}^V G_{in}^\Gamma(r_{N+1}), \tag{2.12}$$

where ${}^V G_{in}^\Gamma$ are reduced radial functions in the velocity gauge. We will not go into the specifics of the outer-region solution here. The reader is instead referred to Burke *et al.* (1991) or Dörr *et al.* (1992). Briefly, a set of coupled differential equations is obtained for the electron in the external region, which is solved subject to boundary conditions at $r = a$ and asymptotically. Combining this with the inner-region solution gives the complete RMF solution for the system.

In recent years, calculations have been carried out on a wide range of atoms and negative ions including H, H^-, He, Ne, Ar, Mg, F^-, Cl^- and Li^-. Figure 1 displays some two- and three-photon rates for the detachment of Li^- at an intensity of 1.0×10^{10} W cm^{-2} (Glass *et al.* 1998). It was found that the structure in the $2s\epsilon\ell$ channel

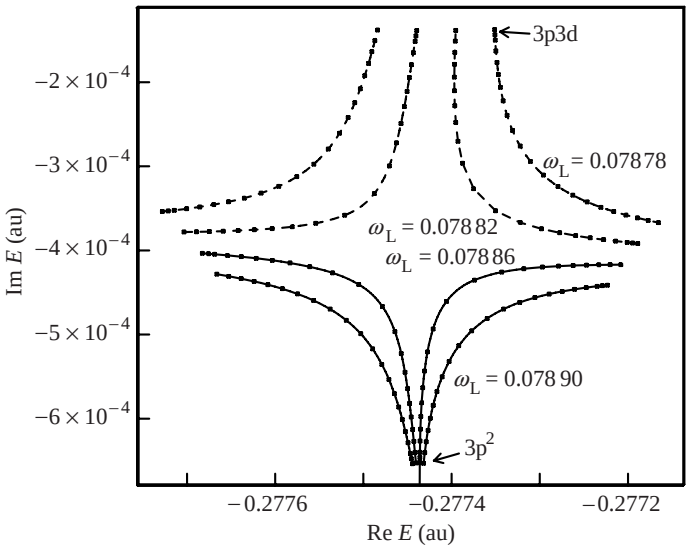

Figure 2. The trajectories of the complex quasi-energies of the 3p3d ^{1}P^o and 3p^2 ^{1}S^e autoionizing states of Mg as a function of the intensity of the second laser as outlined in the text and for the frequencies shown in the figure. The arrows indicate the states at the lowest intensity considered (1.0×10^9 W cm^{-2}).

at a frequency of 0.0484 au disappeared at a lower intensity (see inset). This was explained by a three-photon excitation of a ^{1}P^o resonance near the 3s threshold followed by emission of one photon. This process interferes with the direct two-photon detachment rate. A large enhancement in three-photon absorption was found at a frequency around 0.055 au and was matched by a decrease in the two-photon rate. In this case, one-photon excitation of the residual atom occurs after two-photon detachment has taken place.

In figure 2, two-colour calculations for Mg by Kylstra *et al*. (1998) are considered. The frequency of one laser was tuned to the two-photon resonance between the 3s^2 ground state and a 3p^2 autoionizing state at an intensity of 5.0×10^9 W cm^{-2}. The intensity of a second laser was increased from 1.0×10^9 W cm^{-2} to 5.0×10^9 W cm^{-2} for the different frequencies shown. This laser coupled the 3p^2 and 3p3d autoionizing states, and the figure shows the trajectories of each of these states in the complex energy plane. The trajectories illustrate the existence of a laser-induced degenerate state (LIDS), since, for a certain intensity and frequency, the quasi-energies of the states become identical (corresponding to the middle of the figure).

Harmonic generation has also been studied for a number of cases. Gębarowski *et al*. (1997) investigated third-harmonic generation (THG) in Mg in the vicinity of the three-photon resonance with the 3p3d ^{1}P^o autoionizing state just above the first ionization potential. A large enhancement of the conversion efficiency was observed (figure 3) as the changing laser intensity brought the state into resonance.

Until recently, calculations have required all the eigenvalues and eigenstates of $\boldsymbol{H}_F + \boldsymbol{L}_B$ to be obtained. However, for the study of multiphoton processes at low frequencies and/or high intensities, a large number of Floquet blocks are required to obtain convergence. The *full* diagonalization of the consequently very large $\boldsymbol{H}_F + \boldsymbol{L}_B$

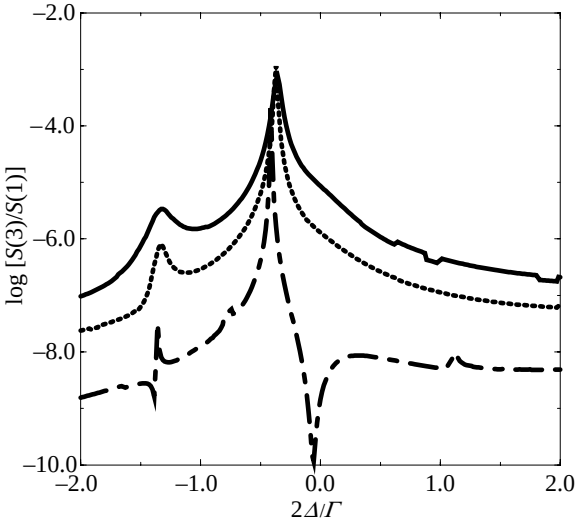

Figure 3. The THG spectrum near the $3p3d\,{}^1P^o$ resonance in Mg at various laser field intensities 1.0×10^{11} W cm^{-2} (solid line), $I=5.0\times10^{10}$ W cm^{-2} (dotted line) and $I=1.0\times10^{10}$ W cm^{-2} (dashed line) versus the scaled detuning $2\Delta/\Gamma=2(\omega-\omega_r)/\Gamma$, where ω_r is the frequency for which there is a three–photon resonance with the autoionizing state, and ω is the laser frequency.

is a prohibitively large computation. Glass *et al*. (1997) have adopted a new approach that exploits the sparsity and periodic nature of the Floquet Hamiltonian to solve a set of linear simultaneous equations instead of performing the diagonalization, a method that is well suited to parallel architectures.

Finally, the reader is referred to Joachain (1996) for a recent review of other calculations (such as those for laser-assisted electron–atom collisions and LIDSs) performed using the RMF method.

(*b*) *Intense-field many-body S-matrix theory*

This approach has been developed by Becker & Faisal (1996) to study non-sequential double ionization in helium. The gist of the method can readily be understood by considering the leading Feynman diagram of the S-matrix series, as shown in figure 4. An initial state comprising an uncorrelated product wave function for the two electrons (denoted by 1 and 2 in the diagram) is used. One of these two electrons interacts with the laser field (denoted by '$-*$') and is promoted into intermediate Volkov states of momenta $\{\boldsymbol{k}\}$, while the second electron propagates in intermediate ionic states, mainly the He^+ ground state. Propagation in these intermediate states is governed by the two-electron Green's function G^0. The two electrons then interact with each other through the Coulombic repulsion term $1/r_{12}$, sharing the energy and angular momenta absorbed by the first electron until both have enough energy to ionize and emerge in final plane wave states with momenta $\{\boldsymbol{k}_a\}$ and $\{\boldsymbol{k}_b\}$.

Using this method, agreement (to within an order of magnitude) with two-electron yields measured experimentally by Walker *et al*. (1994) was reported over a range of intensities up to the saturation intensity.

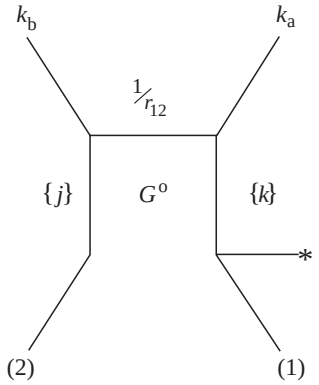

Figure 4. Leading Feynman diagram for double ionization of helium. Time is assumed to flow from the bottom upwards.

3. Time-dependent methods

The direct solution of the TDSE for an atom interacting with a radiation field is a difficult task, especially when multielectron atoms are considered. Most methods involve a number of significant approximations. The simplest of these approaches is the so-called essential states method, in which the atom in the laser field is modelled by a finite number of stationary states entering with time-dependent coefficients. The TDSE in this case reduces to a set of coupled equations for these coefficients that are propagated in time. In § 3 *a* below, we consider this method. The remainder of the section is then devoted to methods that represent the wave function in a more general fashion. After a discussion of one-dimensional models that greatly reduce the complexity of the problem, three-dimensional models are described.

The one- and three-dimensional models generally involve numerical grid methods, in which the atomic wave function is represented on a real-space grid, the whole of which is propagated in time (Kulander 1987*a*). Such an approach is computationally very demanding, since the grid on which the solution propagates must be large enough to contain it for the duration of the laser pulse so that reflections from the edge of the grid do not occur. In deciding the size of the grid to use, account must be taken of the characteristics of the laser pulse imparting energy to the electrons. Modelling the atomic dynamics induced by currently producible short laser pulses can result in large spatial grids. In many cases, absorbing potentials are incorporated to absorb any flux that approaches the edge of the grid. In a recent approach (Scrinzi & Piraux 1997), these problems have been avoided by working with a complex rotated Hamiltonian, for which solutions of the corresponding TDSE can be expressed in terms of L^2 basis functions.

(*a*) *Essential states method*

In this approach, the atom is modelled by a finite number of states, which are coupled together through the interaction with the field. For high-intensity fields, the validity of this approach becomes questionable due to the dissimilarity between the states considered and the actual time-evolving dressed states. Nevertheless, such models have been able to qualitatively assess the contribution of various atomic

states to different multiphoton processes. These models range in complexity from those describing the atom in terms of only two bound states to those describing it in terms of many field-free states (both bound and continuum). It is only the latter extreme that has been useful in the investigation of multielectron atoms. In such cases, a large number of field-free atomic states is expanded on a complete basis of functions within a finite box, the effect of which is to discretize the continuum. Calculations by Lambropoulos and co-workers have used a basis set of B-spline functions. Their method (Tang *et al*. 1990) consists of expanding the field-free hydrogenic eigenfunctions, $\phi_{nlm}(\boldsymbol{r})$, in terms of B-spline functions and spherical harmonics

$$\phi_{nlm}(\boldsymbol{r}) = \sum_{\nu=1}^{N} C_{\nu}^{nlm} B_{\nu}(r) Y_{lm}(\hat{\boldsymbol{r}}). \tag{3.1}$$

The field-free states of a two-electron atom, $\psi_{nLM}(\boldsymbol{r}_1, \boldsymbol{r}_2)$†, are then constructed from antisymmetrized linear combinations of products of these hydrogenic functions. Some (field-free) correlation is included by increasing the number of configurations describing each two-electron state. The time-evolving two-electron wave function in the laser field, $\Psi(\boldsymbol{r}_1, \boldsymbol{r}_2, t)$, is expanded in terms of these field-free two-electron states,

$$\Psi(\boldsymbol{r}_1, \boldsymbol{r}_2, t) = \sum_{nLM} b_{nLM}(t) \psi_{nLM}(\boldsymbol{r}_1, \boldsymbol{r}_2), \tag{3.2}$$

and substitution in the TDSE yields a set of coupled differential equations for the expansion coefficients, namely

$$\mathrm{i}\frac{\mathrm{d}}{\mathrm{d}t} b_{nLM}(t) = \sum_{n'L'M'} \begin{bmatrix} E_{nLM}\delta_{nn'}\delta_{LL'}\delta_{MM'} \\ -\langle \psi_{nLM} \mid V(t) \mid \psi_{n'L'M'} \rangle \end{bmatrix} b_{n'L'M'}(t), \tag{3.3}$$

where E_{nLM} is the energy of the state $|nLM\rangle$, and $V(t)$ is the interaction potential.

Initially, this method was used to study nonlinear susceptibilities and ionization, firstly in helium (Tang *et al*. 1991) and later in alkaline earth atoms (Lambropoulos & Tang 1994), in which case, a length-gauge description of the interaction potential was used. Further studies (Zhang & Lambropoulos 1995) addressed above-threshold ionization (ATI) in helium, in which a velocity-gauge description was used. Electron spectra calculated using this approach were amongst the first full-dimensionality non-perturbative two-electron spectra obtained.

(*b*) *One-dimensional models*

The simplest approach to integrating the TDSE on a numerical grid is to restrict the number of spatial dimensions of each electron to just one. This approach has been applied to two-electron atoms (Pindzola *et al*. 1991; Grobe & Eberly 1992, 1993*a*, *b*; Eberly & Grobe 1994; Haan *et al*. 1994; Lappas *et al*. 1996; Bauer 1997). The field-free Hamiltonian, H_{a}, for such a system has the form

$$H_{\mathrm{a}} = -\sum_{i=1}^{2}\left[\frac{1}{2}\frac{\partial^2}{\partial x_i^2} + V(x_i)\right] + V(x_1, x_2), \tag{3.4}$$

† In this expression, n is an abbreviation for the pair $n_1 n_2$ of principal quantum numbers of the hydrogenic wave functions, L is the total angular momentum quantum number, and M is the total magnetic quantum number.

where x_i is the coordinate of the ith electron, $V(x_i)$ models the attractive Coulomb potential between electron i and the nucleus, and $V(x_1, x_2)$ models the repulsive Coulomb potential between the two electrons. This restriction to one spatial dimension considerably reduces the amount of computer time required to propagate the wave function for the duration of the laser pulse and allows larger excursions through space to be considered. Therefore, the qualitative effect of systematic parameter changes (for instance, to the frequency, intensity and profile of the pulse) can be studied relatively easily, and can shed light on various physical processes. On the other hand, with the one-dimensional restriction, angular momentum effects in the laser-driven atom cannot be investigated. Nor can the effect of circularly and elliptically polarized radiation on the atom be studied.

The Coulomb potential between two particles has a singularity where the position vectors of the particles coincide. In three dimensions, this presents no difficulty because the volume element in three dimensions removes such singularities. But in one-dimensional calculations, a difficulty does arise and this is overcome by replacing the various Coulomb potential terms in equation (3.4) by model potentials, from which such singularities are absent. By far the most widely used potential is the screened Coulomb potential, used initially by Javanainen *et al*. (1988) with the form

$$V(x) = 1/\sqrt{a^2 + x^2}, \tag{3.5}$$

where a is a soft-core parameter. The benefits of this potential are that parity remains a good quantum number† and that the asymptotic behaviour is the same as that of the pure Coulomb potential. As in a real atom, a Rydberg-like series of bound levels having definite parity are supported. The bound-state energies differ from those of the true atomic states. Eberly (1990) has shown that by varying the soft-core parameter, the energy spectrum of bound states can be altered so that the ground-state energy of the model atom coincides with that of the true atom. In describing the Coulomb interaction between electrons, various model potentials have also been used. Several authors (Eberly & Grobe 1994; Pindzola *et al*. 1995) used an extension of the soft-core potential

$$V(x_1, x_2) = 1/\sqrt{a^2 + (x_1 - x_2)^2}, \tag{3.6}$$

whereas Pindzola *et al*. (1991) used a potential having the form

$$V(x_1, x_2) = 1/\sqrt{a_1^2 + x_1^2 + x_2^2 + 2a_2|x_1|\,|x_2|}. \tag{3.7}$$

The main difference in these two potentials lies in their symmetry properties: the potential defined by equation (3.6) is symmetric under rotations of the coordinate system by 180°, whereas the potential defined by equation (3.7) is symmetric under rotations of the coordinate system by 90°.

Lappas *et al*. (1996) have studied correlation effects in a one-dimensional model of the helium atom. In particular, they investigated harmonic generation in the multiphoton regime and multiphoton ionization (MPI) in the tunnelling regime. Their results for harmonic generation demonstrated that for the laser parameters considered (a wavelength of 912 nm and an intensity of 3.5×10^{14} W cm^{-2}), there was

† In fact, it has been suggested that the parity of this potential is a remnant of angular momentum in three dimensions, and that the dipole selection rules are analogous to those in three-dimensions (Javanainen *et al*. 1988).

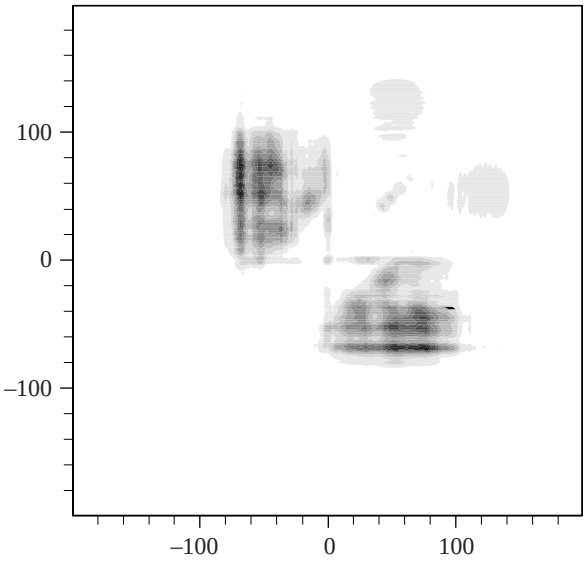

Figure 5. Contour plot of the two-electron joint probability distribution after five optical cycles of a six-cycle laser pulse having a wavelength of 912 nm and a peak intensity of 1.0×10^{15} W cm^{-2}. The length-scales on both axes are in atomic units.

negligible contribution from the ionic core. On the other hand, plots of the joint two-electron probability distribution (at an intensity of 1.0×10^{15} W cm^{-2}) showed clear evidence of correlated double ionization. Figure 5 is such a plot made after five optical cycles of a six-cycle laser pulse. In this plot, single-electron excitation and ionization are observed to occur as well as correlated double-electron ionization. However, a study of the time evolution of the electron probability density was not undertaken in that work.

(*c*) *Three-dimensional models*

The solution of the TDSE in three dimensions is significantly more demanding computationally than in one dimension. Until recently, such an approach was not possible for two-electron atoms without making a number of severe approximations. In this section, we will describe some of these approximations, namely the time-dependent Hartree–Fock method, density functional theory, and the single-active-electron approximation plus extensions. We then go on to describe methods that handle a two-electron atom in its full dimensionality and, finally, outline a new method, namely the time-dependent *R*-matrix approach, applicable, in principle, to a general multielectron atom.

(i) *Time-dependent Hartree–Fock*

The time-dependent Hartree–Fock (TDHF) method (or time-dependent self-consistent field method) has recently been applied by Kulander (1987*b*, 1988) in order to study multiphoton processes in multi-electron atoms. In this approach, the time evolution of the electronic orbitals is followed using the mean field of the total electron density as part of a time-dependent potential. In this way, some of the instantaneous

correlation of the electrons is smeared out or averaged over, while the rest of the interactions are handled accurately. This mean-field approximation reduces the complexity of the problem from one of solving the TDSE for the $3N$-dimensional wave function of an N-electron atom to one of solving a set of three-dimensional equations for the N orbitals.

Originally, Kulander (1987*b*) expanded the wave function Ψ of the N-electron system as a single Slater determinant:

$$\Psi(\boldsymbol{r}_1,\ldots,\boldsymbol{r}_N,t)=\mathcal{A}\prod_{i=1}^{N}\varphi_i(\boldsymbol{r}_i,t), \tag{3.8}$$

where $\mathcal{A}$ is the antisymmetrization operator, φ_i is a single-electron orbital, and $\boldsymbol{r}_i$ is the position vector of electron i. Substituting this into the TDSE yields

$$\mathrm{i}\frac{\partial}{\partial t}\varphi_i(\boldsymbol{r}_i,t)=\left[-\tfrac{1}{2}\nabla_i^2+\sum_j\int \mathrm{d}\boldsymbol{r}_j\frac{|\varphi_j(\boldsymbol{r}_j,t)|^2}{|\boldsymbol{r}_i-\boldsymbol{r}_j|}-\left(\frac{Z}{r_i}\right)-z_i\varepsilon_0 f(t)\sin\omega_0 t\right]\varphi_i(\boldsymbol{r}_i,t)$$
$$-\sum_{i\neq j}\left\{\int \mathrm{d}\boldsymbol{r}_j\frac{\varphi_i^{\star}(\boldsymbol{r}_i,t)\varphi_j(\boldsymbol{r}_j,t)}{|\boldsymbol{r}_i-\boldsymbol{r}_j|}\right\}\varphi_j(\boldsymbol{r}_j,t), \tag{3.9}$$

where a length-gauge description has been used. A number of problems with this method immediately arise as follows.

(1) The exchange potential (entering the final term) must be evaluated for each orbital, a calculation that presents the principal computational difficulty of the method. However, as in field-free Hartree–Fock theory, it is possible to define the exchange potential in terms of a fictitious exchange charge density that will have certain features common to all the occupied orbitals. Thus, an average exchange potential can be defined, representative of all occupied orbitals. This gives rise to the local density approximation (LDA) valid provided the exchange forces are not very large (Hermann & Skillman 1963).

(2) Since only a single configuration is retained, the autoionization process is absent from this model. Moreover, if only a single spatial orbital is retained (Kulander 1987*b*), the final state of the system is not well defined. This can be seen in the case of helium by writing the doubly occupied orbital as

$$\varphi(\boldsymbol{r},t)=a_{1\mathrm{s}}(t)\varphi_{1\mathrm{s}}(\boldsymbol{r})+a_{kl}(t)\varphi_{kl}(\boldsymbol{r}), \tag{3.10}$$

where $\varphi_{1\mathrm{s}}(\boldsymbol{r})$ is the ground-state orbital, and $\varphi_{kl}(\boldsymbol{r})$ is an excited-state orbital entering with time-dependent coefficients $a_{1\mathrm{s}}(t)$ and $a_{kl}(t)$, respectively. In this case, the probability for single ionization, $2\,\mathrm{Re}(a_{1\mathrm{s}}^{*}a_{kl})$, is related to the probability for double ionization, $|a_{kl}|^2$, leading to the unphysical constraint that there cannot be substantial single ionization without double ionization occurring. Several authors have relaxed the multiply occupied orbital constraint. Horbatsch *et al*. used the unsymmetrized representation

$$\Psi(\boldsymbol{r}_1,\boldsymbol{r}_2,t)=\phi(\boldsymbol{r}_1,t)\chi(\boldsymbol{r}_2,t), \tag{3.11}$$

to study photoionization (Horbatsch *et al*. 1992) and harmonic generation (Horbatsch 1994) in helium. This unsymmetrized representation is unphysical, since it allows the two electrons to be distinguished. Pindzola *et al*. (1995)

used the fully symmetrized representation

$$\Psi(\boldsymbol{r}_1, \boldsymbol{r}_2, t) = (1/\sqrt{2})[\phi(\boldsymbol{r}_1, t)\chi(\boldsymbol{r}_2, t) + \phi(\boldsymbol{r}_2, t)\chi(\boldsymbol{r}_1, t)]. \tag{3.12}$$

However, as in their earlier studies (Pindzola *et al*. 1991), the number of spatial dimensions of each electron was reduced from three to one, in order to make the calculation manageable on the computer resources available.

(3) The main drawback with the TDHF method comes about through the Coulomb and exchange potentials in equation (3.9) depending on the occupation numbers of the various orbitals. The linear TDSE gets transformed into a set of non-linear equations that tend to inhibit ionization. Upon ionization, the electron density in the vicinity of the nucleus decreases so that the orbital occupation is decreased. The mean field experienced by each electron, therefore, decreases, leading to a reduced screening of the nucleus, which, in turn, increases the binding energy of the atom. Population trapping results, and so it is not possible† to assign an accurate ionization rate. This can be seen in figure 6, where the helium ionization rates calculated by Pindzola *et al*. (1995) are plotted. Four different cases were considered, namely a one-dimensional numerical grid calculation, a one-dimensional TDHF calculation using a multiply occupied orbital (equation (3.8)), a one-dimensional TDHF frozen-core calculation using a multiply occupied orbital, and a one-dimensional TDHF calculation using a fully symmetrized wave function consisting of two orbitals (equation (3.12)).

(ii) *Time-dependent density functional theory*

Density functional theory (DFT), as first introduced by Hohenberg & Kohn (1964) and Kohn & Sham (1965), describes a system of interacting particles in terms of its density. The theory is based on the existence of an exact mapping between densities and external potentials and leads to the density of the interacting system being obtained from the density of an auxiliary system of non-interacting particles moving in an effective local single-particle potential, i.e. the particle interactions are treated in an averaged-over manner.

A time-dependent formalism of DFT (TDDFT) was provided by Runge & Gross (1984), who showed that the time-dependent density could be obtained from the response of non-interacting particles to the time-dependent local effective potential

$$v_{\mathrm{s}}(\boldsymbol{r}, t) = v(\boldsymbol{r}, t) + \int \mathrm{d}\boldsymbol{r}' \frac{n(\boldsymbol{r}', t)}{|\boldsymbol{r} - \boldsymbol{r}'|} + v_{xc}(\boldsymbol{r}, t). \tag{3.13}$$

In this expression, the first terms on the right-hand side represent, respectively, the external potential, the Hartree potential and the local exchange-correlation potential. Expanding the total wave function of the N-particle system as a Slater determinant of single-electron orbitals, $\varphi_j(\boldsymbol{r}, t)$, results in the density, $n(\boldsymbol{r}, t)$, being given by

$$n(\boldsymbol{r}, t) = \sum_{j=1}^{N} |\varphi_j(\boldsymbol{r}, t)|^2. \tag{3.14}$$

† Apart from low intensities when the nonlinearity is less pronounced.

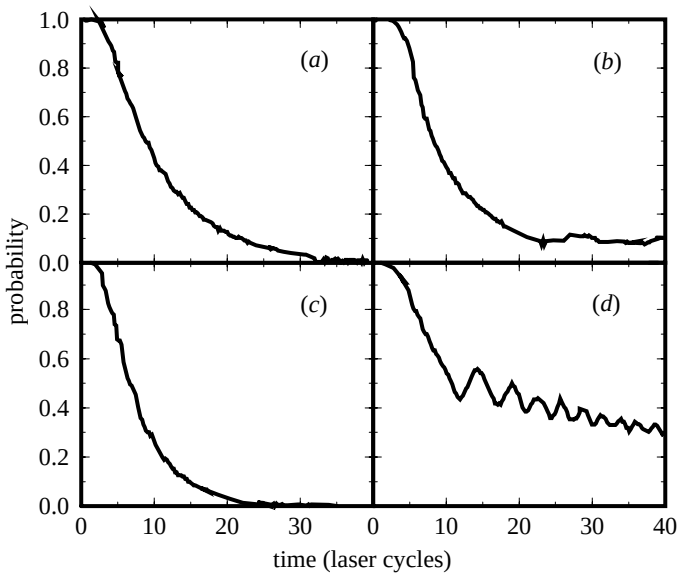

Figure 6. Time evolution of the ground-state probability for three-photon ionization of the model helium atom at an intensity of 1.0×10^{15} W cm^{-2}. The decay curves correspond to (*a*) a one-dimensional numerical grid calculation, (*b*) a one-dimensional TDHF calculation using a multiply occupied orbital, (*c*) a one-dimensional TDHF frozen-core calculation using a multiply occupied orbital, and (*d*) a one-dimensional TDHF calculation using a fully symmetrized wave function consisting of two orbitals.

In analogy with the static case, these orbitals satisfy time-dependent Kohn–Sham type equations

$$\mathrm{i}\frac{\partial}{\partial t}\varphi_j(\boldsymbol{r},t) = (-\tfrac{1}{2}\boldsymbol{\nabla}^2 + v_\mathrm{s}[n](\boldsymbol{r},t))\varphi_j(\boldsymbol{r},t), \tag{3.15}$$

where

$$v_\mathrm{s}[n](\boldsymbol{r},t) = v(\boldsymbol{r},t) + \int \mathrm{d}\boldsymbol{r}'\,\frac{n(\boldsymbol{r}',t)}{|\boldsymbol{r}-\boldsymbol{r}'|} + v_{xc}[n](\boldsymbol{r},t) \tag{3.16}$$

is the effective potential functional of the density, which defines a time-dependent exchange-correlation potential (Gross *et al*. 1996). In principle, the averaged-over many-body effects can be included exactly through the exchange-correlation term, but in practice, these effects have to be approximated. Two approximation schemes have generally been employed. The first of these is simply the LDA, which was described for the TDHF method. In the time-dependent case, this approximation will only be valid if the time dependence of the density is sufficiently slow, i.e. that it responds adiabatically. In addition, the LDA contains self-interaction contributions that must be removed in order to obtain good potentials. The second scheme is a time-dependent version of the optimized potential method (TDOPM) (Sharp & Horton 1953; Talman & Shadwick 1976), which results in a potential free from self-interactions. A full description of the method is given by Ullrich *et al*. (1995*a*). The local effective potential defined by equation (3.13) is chosen so that the orbitals obtained by solving the time-dependent Kohn–Sham equations (defined by equa-

tion (3.15)), up to a time t_1, render the total action functional,

$$\mathcal{A}[\varphi_1 \cdots \varphi_N] = \sum_{j=1}^{N} \int_{-\infty}^{t_1} \mathrm{d}t \left\langle \varphi_j(\boldsymbol{r},t) \middle| \left(\mathrm{i}\frac{\partial}{\partial t} + \tfrac{1}{2}\boldsymbol{\nabla}^2 - v_\mathrm{s}(\boldsymbol{r},t) \right) \middle| \varphi_j(\boldsymbol{r},t) \right\rangle, \qquad (3.17)$$

stationary. This leads to the solution of an integral equation that is computationally demanding. Making a KLI transformation introduced by Krieger *et al*. (1990) leads to an alternative, but still exact, form of the TDOPM, which no longer involves the solution of the integral equation (Ullrich *et al*. 1995*a*) and is known as the TDKLI approximation.

TDDFT is, structurally, very similar to the TDHF method described earlier, and, therefore, it suffers from the same drawbacks. It is, however, computationally less demanding, since it does not include non-local potentials. In addition, Ullrich *et al*. (1995*a*) point out that experience with DFT suggests that the results obtained from the TDOPM and from the TDKLI approximation should agree well with the non-local TDHF results in the exchange-only limit. They further point out that correlation effects can be included approximately through various model potentials with no additional numerical effort.

Using this method in the exchange only limit, the interaction of various multielectron atoms has been studied in the presence of intense laser pulses (Ullrich *et al*. 1995*b*; Gross *et al*. 1996). In general, the time-evolution of several multiply occupied orbitals has been calculated. For instance, Gross *et al*. (1996) determined the time-evolution of the 2s, $2p_0$ and $2p_1$ orbitals in neon for a 248 nm pulse, which linearly ramped up over 10 optical cycles to a peak intensity of 3.0×10^{15} W cm^{-2}. From this, they were able to estimate populations for the first three charged states of neon. However, it has been pointed out by Bauer (1997) that such an approach results in inaccurate estimates, since physical relevance is assigned to the orbitals. In principle, the ion yields can be obtained as functionals of the density, although this is quite difficult in practice. Further work (Erhard & Gross 1996; Lappas & van Leeuwen 1998) has incorporated correlation potentials to study the influence of correlation beyond the TDHF method.

(iii) *Single active electron and beyond*

We saw earlier how the nonlinearity of the TDHF equations leads to reduced ionization rates. In order to redress this problem, Kulander (1987*b*) introduced the 'frozen-core' approximation, in which only one-electron orbital is allowed to respond to the field. Assuming that the response to the field is just a small distortion of field-free orbitals so that

$$\varphi_i(\boldsymbol{r}_i,t) = \phi_i(\boldsymbol{r}_i) + \delta(\boldsymbol{r}_i,t), \qquad (3.18)$$

where the ϕ_i represent the field-free Hartree–Fock orbitals of the atom, then the leading terms in the wave function expansion are

$$\Psi(\boldsymbol{r}_1,\ldots,\boldsymbol{r}_n,t) \simeq \mathcal{A}\sum_j (\phi_j(\boldsymbol{r}_j) + \delta_j(\boldsymbol{r}_j,t)) \prod_{i\neq j} \phi_i(\boldsymbol{r}_i). \qquad (3.19)$$

Substituting this expression into the TDHF equation (equation (3.9)) and retaining terms to first order in the resulting TDSE, results in an equation that describes a single active electron (SAE) moving in response to the field in the time-independent

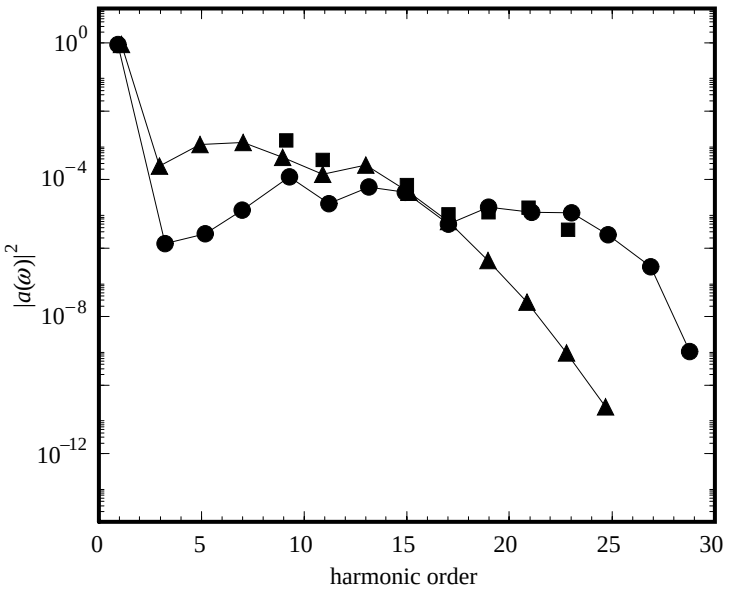

Figure 7. Theoretical harmonic response for He (triangles) and He^+ (circles) irradiated by a 248 nm pulse of duration 105 fs and peak intensity 3.2×10^{15} W cm^{-2}, compared with the experimental response (squares). The experimental data have been normalized to the 13th harmonic.

field of the other electrons assumed to be in their ground-state orbitals. Thus, only this active electron experiences the external field. This simplification means solving a set of linear equations. However, as with the TDHF method, information about the correlation between the electrons is not included explicitly but is, instead, included through the initial state in an averaged-over manner. Furthermore, as in the RMF method, multiple excitation can only be modelled by assuming that the electrons are ionized sequentially.

Sanpera *et al*. (1995) studied harmonic generation beyond the saturation intensity in helium using the SAE approach, whereby the effective time-independent potential was constructed from Hartree calculations on the helium ground state. They expanded the wave function of the active electron over an angular basis with the radial part represented on a numerical grid of $300a_0$ in extent, with a mesh spacing of $0.1a_0$. Results for harmonic generation were compared with those obtained experimentally using a 248 nm pulse of duration 105 fs and peak intensity 3.2×10^{15} W cm^{-2}, as presented in figure 7. Good agreement between the experimental and calculated data was found. Preston *et al*. (1996) also calculated harmonic generation in helium using an SAE calculation and used a one-dimensional SAE calculation to model the different ionization stages of neon. Kulander and co-workers (Kulander *et al*. 1992; Krause *et al*. 1992) have calculated harmonic spectra for all the rare gases using full three-dimensional SAE calculations with appropriate effective potentials, and they found good qualitative agreement with the macroscopic conversion efficiencies obtained experimentally by Li *et al*. (1989).

Watson *et al*. (1997) have recently proposed an extension to the SAE model in helium, allowing the inner electron to experience a time-dependent potential repre-

senting the effect on it of the outer one. In this method, the wave function of the two-electron atom is written as the product of one-electron orbitals

$$\Psi(\boldsymbol{r}_1, \boldsymbol{r}_2, t) = (1/\sqrt{2})[\psi_i(\boldsymbol{r}_1, t)\psi_o(\boldsymbol{r}_2, t) + \psi_i(\boldsymbol{r}_2, t)\psi_o(\boldsymbol{r}_1, t)]. \tag{3.20}$$

Assuming the overlap between the two electrons to be small means the exchange interaction between them can be neglected and, hence, only the first term on the right-hand side of the equation needs to be retained. It is thus possible to distinguish the inner electron from the outer electron (denoted, respectively, by the subscripts i and o). As in the SAE approximation, the outer electron experiences the time-independent Hartree–Fock potential due to the inner electron. The frozen constraint on the inner electron is then removed, allowing it to move in the time-dependent mean field due to the outer electron and the nucleus, written as

$$V_i(\boldsymbol{r}_1, t) = -\frac{2}{r_1} + \int \frac{\psi_o^*(\boldsymbol{r}_2, t)\psi_o(\boldsymbol{r}_2, t)}{|\boldsymbol{r}_1 - \boldsymbol{r}_2|}\, \mathrm{d}\boldsymbol{r}_2. \tag{3.21}$$

With such a model, it has been possible to include some correlation between the two electrons. Indeed, as illustrated in figure 8, studies with this model have been able to reproduce the knee in plots of double-ionization yield versus intensity, indicating collective response of the electrons.

(iv) *Full treatment of a two-electron atom*

Over the last few years, steadily rising computer power has made possible the solution of the TDSE for a laser-driven two-electron atom, where both electrons are treated on an equal footing and in their full-dimensionality (Parker *et al*. 1996; Taylor *et al*. 1996, 1997; Scrinzi & Piraux 1997). Two distinct approaches have been developed. In the first (Parker *et al*. 1996; Taylor *et al*. 1996, 1997), the TDSE is solved using a mixed basis set, finite-difference method, whereas in the second (Scrinzi & Piraux 1997), a basis of two-electron correlated L^2 functions is used to solve the TDSE after the radial coordinates in its Hamiltonian have been subjected to a rotation in the complex plane.

In the first approach, the radial coordinates r_1 and r_2 of the two electrons are modelled on a finite-difference grid, and the four angular coordinates $(\theta_1, \theta_2, \phi_1, \phi_2)$ are handled by writing the wave function on a basis set of coupled spherical harmonics (partial waves), $|l_1 l_2 L M\rangle$. In linearly polarized light, the z-component of the total angular momentum, M, is constant, resulting in only five independent spatial dimensions. Since the initial state has $M = 0$, the wave function $\Psi(\boldsymbol{r}_1, \boldsymbol{r}_2, t)$ can be written as

$$\Psi(\boldsymbol{r}_1, \boldsymbol{r}_2, t) = \mathcal{A} \sum_{l_1 l_2 L} f_{l_1 l_2 L}(r_1, r_2, t)|l_1 l_2 L\rangle, \tag{3.22}$$

where $\mathcal{A}$ is the Pauli symmetrization operator. Electron spin S is conserved: with the atom in its ground singlet state, its overall spin remains zero, so that $\mathcal{A}$ enforces even symmetry of the wave function under exchange of electron spatial coordinates.

The radiation field, included in the calculations via the velocity gauge, can exchange angular momentum with the electrons, and the number of partial waves coming into play can become quite large. The largest number of partial waves used to date is 385. With this setting, the TDSE becomes a set of 385 coupled two-dimensional time-dependent partial differential equations, each of which is solved

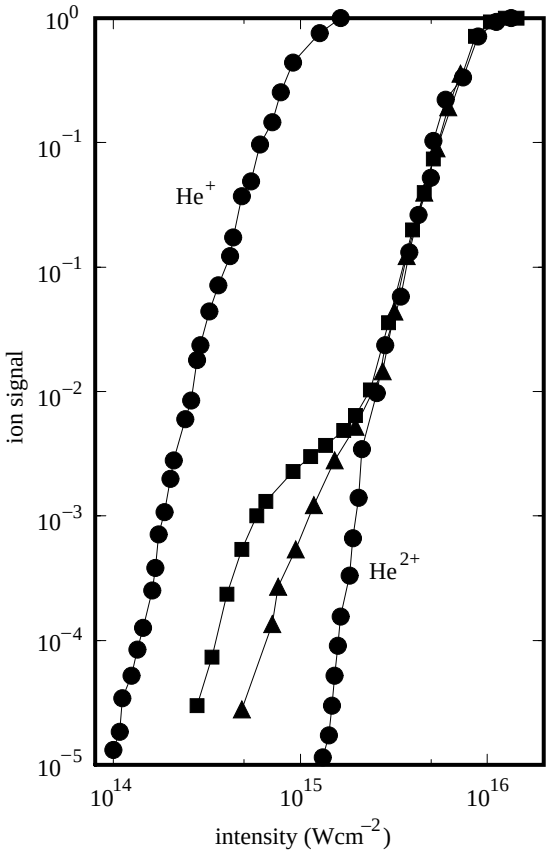

Figure 8. Numerically calculated single- and double-ionization yields from helium calculated in three dimensions for a 780 nm laser pulse of duration 120 fs. The circles correspond to an SAE calculation, while the squares and triangles correspond to the non-sequential model of Watson *et al*. (1997). The triangles correspond to the case where an absorbing boundary was used to inhibit the recollision of the outer electron.

by finite-difference techniques. The kinetic energy operators of the atomic Hamiltonian are approximated as five-point finite-difference operators. The momentum operators of the (velocity-gauge) interaction Hamiltonian are approximated as two- or four-point finite-difference operators. The electron–electron Coulomb potential is expanded in the well-known series:

$$\frac{1}{|\boldsymbol{r}_1 - \boldsymbol{r}_2|} = \frac{1}{r_>} \sum_l \left(\frac{r_<}{r_>} \right)^l P_l(\cos\theta_{12}), \tag{3.23}$$

and a limited number of terms are retained. Two-point finite-difference operators are used to represent the interaction Hamiltonian. The ground state of the finite-difference grid is found by using the Lanczos method to obtain an initial estimate of the eigenvector and, subsequently, propagating the TDSE in imaginary time so that it runs as a diffusion equation, rather than as a wave equation. States of higher energy than the ground state dissipate rapidly (Smyth *et al*. 1998).

The basis state decomposition is particularly well suited to parallelization. The present version of the code runs well on a Cray T3D. At present, the partial waves are mapped onto 256 processors of the Cray T3D. On the T3D, a typical 15 field-period run (consisting of a sinusoidal ramp-up of between two and four cycles to peak intensity, which is maintained for another 5–10 cycles) using 256 processors now takes about five wall-clock hours, assuming 600 time-steps per field period. The results discussed here were obtained in a $100a_0$ box in r_1 and r_2. An absorbing potential at the outer boundary is not used, but rather the wave function is split into a coherent superposition of an outer part and an inner part. The outer part is zero at $r_1, r_2 \leqslant 60a_0$, but grows so that it contains the total wave function at the $100a_0$ boundary, with the consequence that the inner part smoothly approaches zero at the boundary. At present, this outer part is discarded and so the net effect is equivalent to that of an absorbing boundary.

This numerical method is thus capable of faithfully modelling double ionization, autoionization, or any other effect associated with highly correlated states of the two electrons. The degree to which the numerical integration approximates the TDSE is governed by four parameters in the code: the spacing, δr, of the finite-difference grid points representing the two radial variables; the maximum angular momentum, $L_{\max}$, present in the partial-wave expansion; the number of terms retained in a series expansion of the electron–electron interaction; and the size of the integration volume. By changing these parameters, the model can be made arbitrarily close to the TDSE from which it is derived. In the data presented here, the dominant source of error is the rough radial grid. The grid spacing, δr, is set to 0.33 Bohr radii, a setting chosen to economize CPU usage.

Initial results for single-atom processes have already been presented elsewhere (Parker *et al*. 1996, 1998; Taylor *et al*. 1996, 1997) and include ionization populations, harmonic generation rates and visualizations of various aspects of the two-electron probability density. Over the past two years, development and refinement of the algorithms and numerical methods (Smyth *et al*. 1998) has allowed the calculations to progress from semi-quantitative to fully quantitative in quality. For instance, at lower intensities, these calculations have recently (Parker *et al*. 1998) been used to assess the accuracy of single-active-electron models. Figure 9 displays results from the full finite-difference helium calculation (labelled helium) at $\omega = 0.21$ au, as well as from three different SAE models. The dashed–dotted line represents the predictions of a Coulomb potential whose ionization potential has been adjusted to be the same as that of single-electron ionization of helium (0.9037 au). The dashed line gives the predictions of time-dependent Hartree–Fock. The dotted line represents the predictions of a new SAE model introduced by Parker *et al*. (1998). The slopes of the curves are proportional to the instantaneous rate of depletion of populations within eight Bohr radii of the nucleus. The fact that negligible population returns to this inner region after the pulse has been ramped off confirms that this depletion of population is due to ionization. At this relatively low intensity (5×10^{13} W cm^{-2}), the AC Stark shifts are small enough that the comparison can be made without modifying the one-electron SAE models so that they have the same AC Stark shift as the two-electron atom.

Since both electrons of the atom are treated on an equal footing, the method is particularly interesting to apply where laser intensities are such as to bring about ionization of both electrons. Before discussing some illustrative results, it is useful

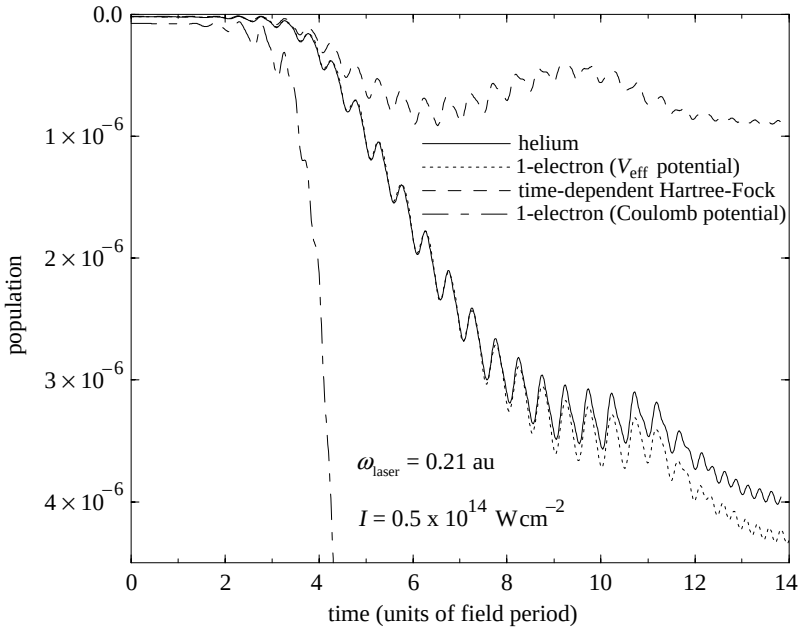

Figure 9. Ionization profiles during a 14 field-period pulse for helium and for three single-active-electron models. The curves show populations eight Bohr radii from the nucleus and beyond during excitation. The pulse is ramped on over four field periods and ramped off similarly.

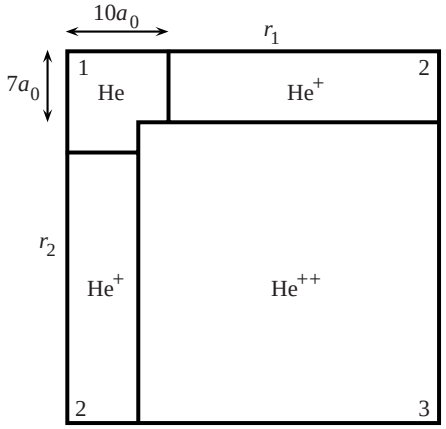

Figure 10. The finite-difference radial grid showing the regions associated with the different charge states in helium. Region 1 corresponds to neutral helium, region 2 to singly excited and singly ionized helium, and region 3 to doubly excited and doubly ionized helium.

to identify specific regions of the two-electron radial space with particular ionization stages of the two-electron atom. This can be seen in figure 10 (see also Dundas *et al.* 1999*a*). Region 1 encompasses the innermost part of the two-electron wave function and is associated with neutral helium. Ground-state helium lies almost entirely within this region. Region 2, where one radial coordinate is large and the other small, mostly

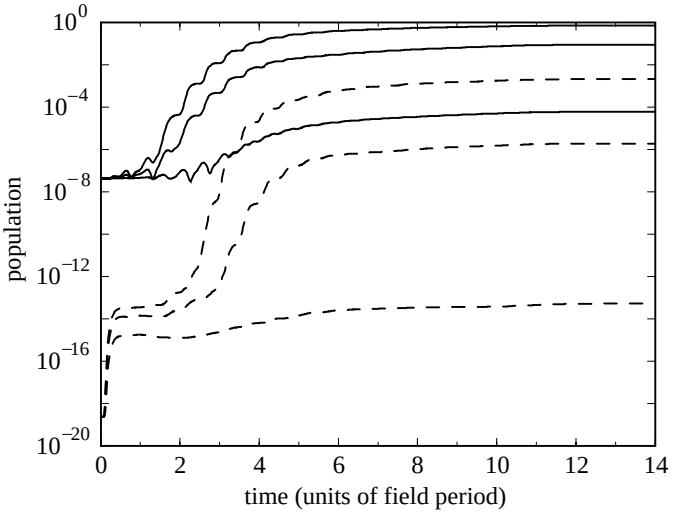

Figure 11. Single and double ionization yields from helium. The laser pulse has a wavelength of 248.6 nm. Solid lines indicate singly ionized population, dashed lines indicate doubly ionized population. Both populations rise steadily with increasing laser intensity and results are given for 1.0×10^{14} W cm^{-2}, 8.0×10^{14} W cm^{-2} and 2.0×10^{15} W cm^{-2}.

contains that part of the wave function where singly excited and singly ionized states of helium are to be found. Region 3, where both radial coordinates are large, is where doubly excited and doubly ionized states of helium are largely located. Movement of electron flux from region 1 to region 2 involves the radial coordinate of one electron increasing, and corresponds to single-electron excitation and ionization of the atom; from region 1 directly to region 3 corresponds to non-sequential double-electron excitation and ionization. Finally, movement from region 2 to region 3 indicates both second-electron excitation and second-electron ionization of already singly excited or singly ionized helium, i.e. sequential double-electron excitation and ionization. Integrating the probability density over both electron coordinates gives a measure of the total population within each ionization stage. Single and double ionization yields are illustrated in figure 11 from calculations for 248.6 nm laser radiation at a number of peak intensities (Parker *et al*. 1998*b*). The laser pulse is ramped on sinusoidally over four cycles, peak intensity is maintained for six cycles, and the pulse is ramped off sinusoidally over four cycles. From this figure, it can clearly be seen how the single- and double-electron ionization yields increase steadily with increasing intensity.

Plots of harmonic generation spectra (Parker *et al*. 1999) are given in figure 12 for the same laser pulses in figure 11. It can clearly be seen how higher laser intensities give rise to higher-order harmonics. In addition, the formation of the plateau region in the spectrum for the highest intensity is clearly visible.

In order to gain more insight into the dynamics underlying these results, a number of visualizations were developed that allowed the time-evolution of the five-dimensional wave function to be followed. In practice, this amounted to taking a two-dimensional cut, with the other dimensions essentially integrated over. By producing radial plots of the joint two-electron probability density, the flux of population between different regions of the grid defined in figure 10 could be studied (Taylor *et al*. 1996, 1997; Dundas *et al*. 1999*b*). Figure 13 displays radial plots at four time-instants

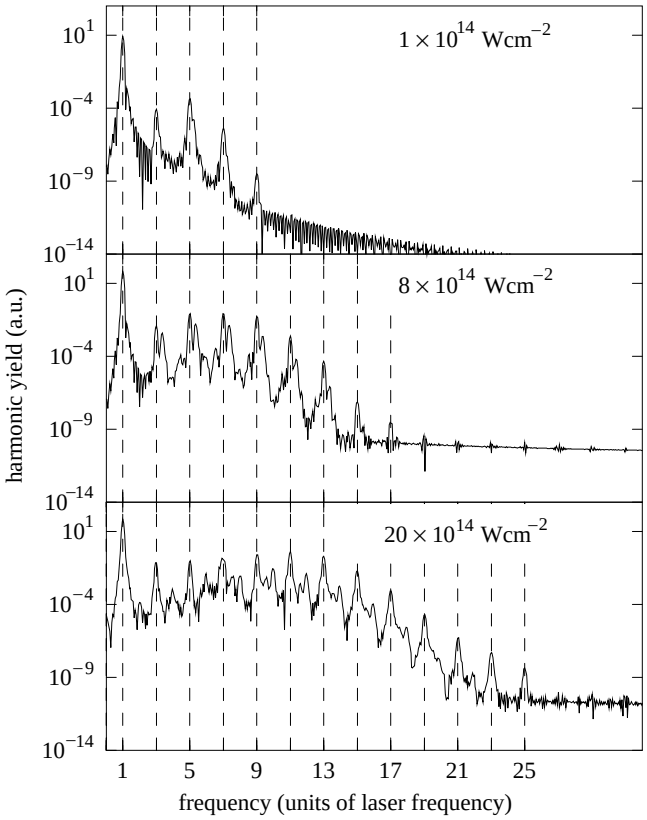

Figure 12. Harmonic generation in helium. The laser pulse has a wavelength of 248.6 nm and the three values of laser peak intensity are the same as in figure 11. Harmonic generation in helium. The laser pulse has a wavelength of 248.6 nm and the three values of laser peak intensity are the same as in figure 11.

during a pulse, rising to a maximum intensity of 8.0×10^{15} W cm^{-2}. In figure 13*a*, at an instant during the initial ramp on, only single-electron excitation and ionization were observed, indicated by a population in region 2. In figure 13*b*, where the field has ramped on fully, a packet has entered region 3 from region 1, indicating the onset of simultaneous double-electron ionization and excitation. In figure 13*c*, shortly after the field has passed through a maximum, sequential double-electron excitation and ionization are also occurring, as indicated by wavefronts passing from region 2 to region 3. In figure 13*d*, roughly one cycle later, further bursts of population moving from regions 1 and 2 to region 3 indicate both further simultaneous and sequential double-electron ionization and excitation.

In order to unambiguously identify the role of the $1/r_{12}$ term in these excitation and ionization pathways, the calculation was repeated dropping this term from the Hamiltonian. Figure 14 displays radial plots from this calculation. Although single-electron excitation and ionization and sequential double-electron excitation and ionization are clearly observed here, the absence of any burst of population migrating from region 1 to region 3 indicates the entire absence of simultaneous double-electron ionization and excitation in this case.

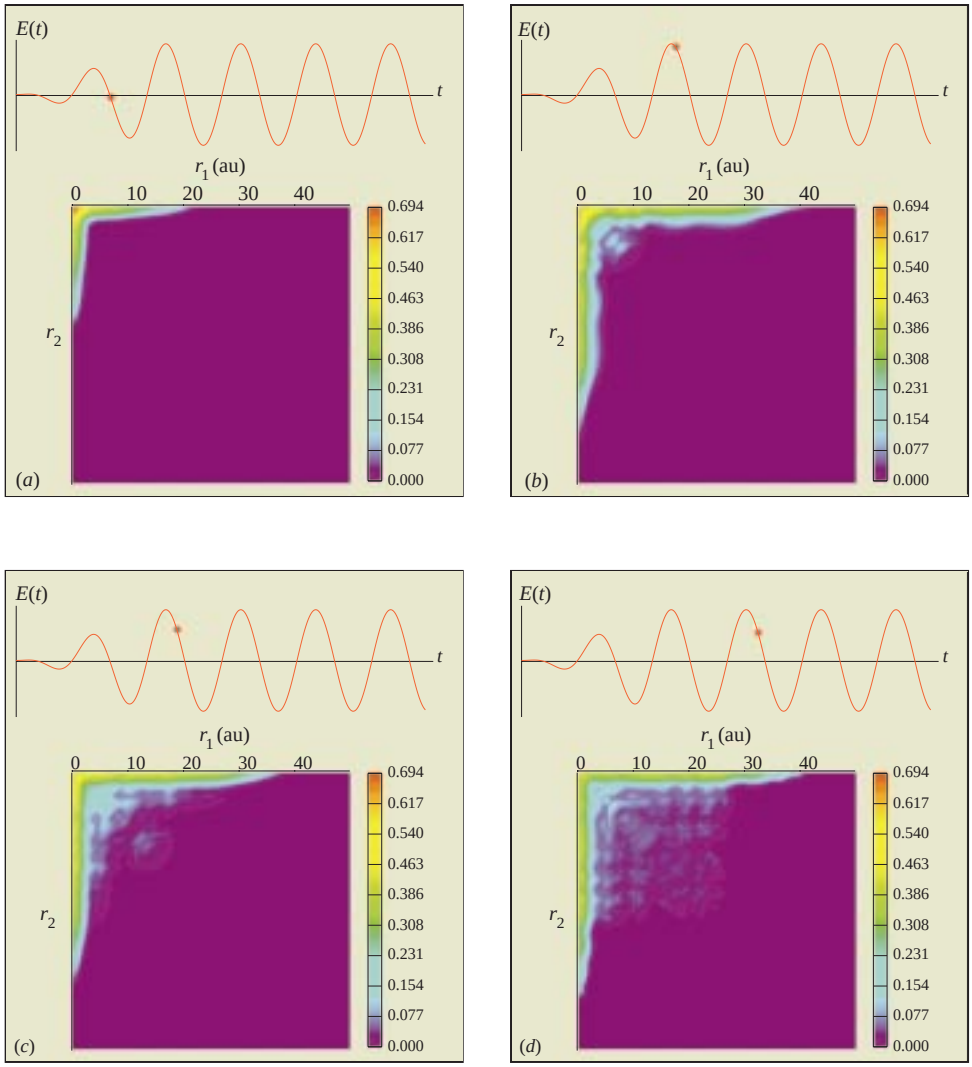

Figure 13. Radial plots of the joint two-electron probability density for a laser pulse of frequency 0.236 au, which ramps up over two optical cycles to a peak intensity of 8.0×10^{15} W cm^{-2}, after which the intensity is held constant for another three cycles. The length-scales on all axes are identical and are in atomic units.

In the alternative approach developed by Scrinzi & Piraux (1997), the starting point was to subject each of the two radial coordinates in the Hamiltonian to a rotation in the complex plane, characterized by the angle θ below. The advantage in doing this is that the solution of the correspondingly altered TDSE can be represented entirely in terms of L^2-type basis functions. This avoids the problems normally associated with cutting off the asymptotically finite oscillatory wave function solution to the true TDSE. Various measurable properties of the true physical system, such as harmonic generation spectra, can be readily obtained from the propagation in time of the wave function solution to this modified TDSE.

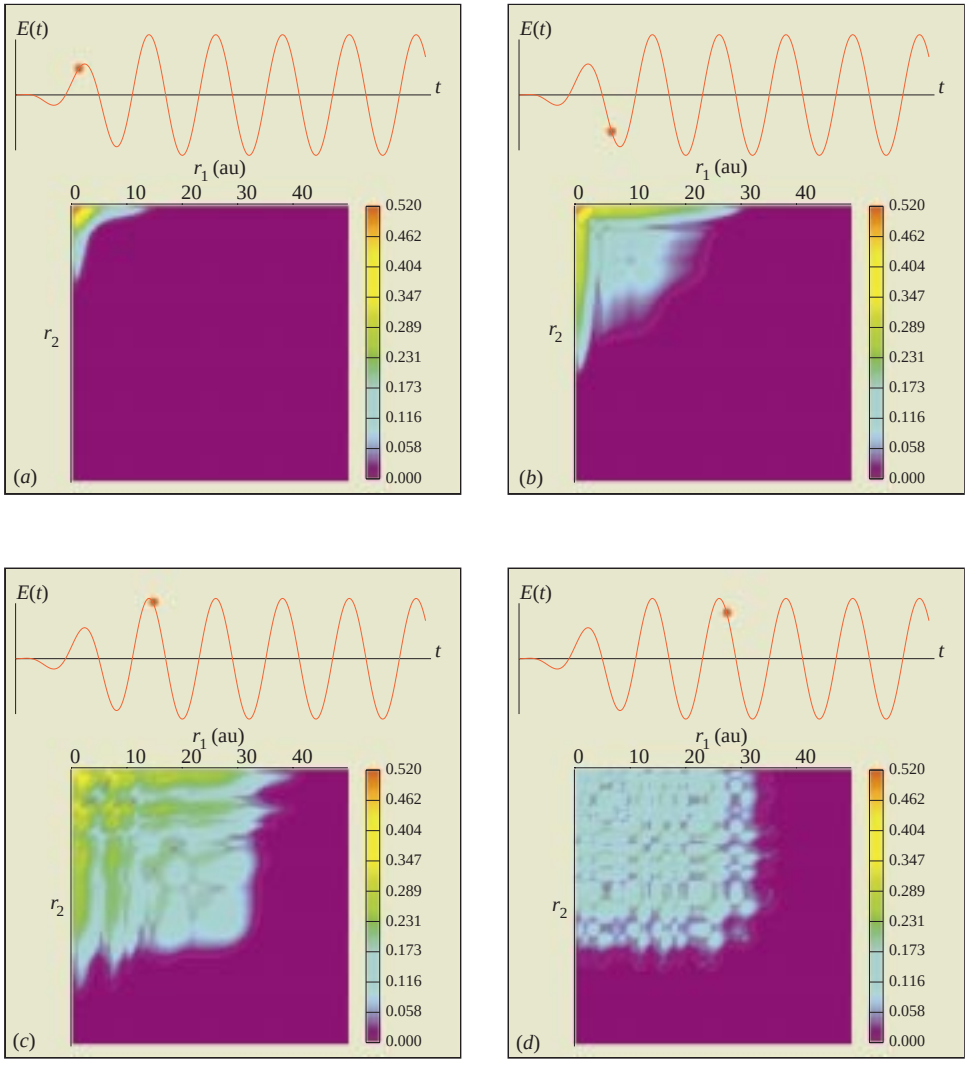

Figure 14. Uncorrelated radial plots of the joint two-electron probability density for a laser pulse of frequency 0.236 au, which ramps up over two optical cycles to a peak intensity of 8.0×10^{15} W cm^{-2}, after which the intensity is held constant for another four cycles. The length-scales on all axes are identical and are in atomic units.

The wave function solution $\Psi_\theta(\boldsymbol{r}_1, \boldsymbol{r}_2, t)$ to the rotated TDSE is expanded over a Hylleras-like explicitly correlated basis:

$$\Psi_\theta(\boldsymbol{r}_1, \boldsymbol{r}_2, t) = \tfrac{1}{2}(1 + P_{12}) \sum_{L=0}^{L_{\max}} \sum_{l_1=0}^{L} G_{Ll_1}(\boldsymbol{r}_1, \boldsymbol{r}_2) \times \sum_i c_i^{Ll_1}(\theta, t) r_1^{k_i} r_2^{m_i} |\boldsymbol{r}_1 - \boldsymbol{r}_2|^{n_i} \exp(-\alpha_i r_i - \beta_i r_2). \quad (3.24)$$

The operator $\frac{1}{2}(1+P_{12})$ projects onto the singlet states, the only species coming into

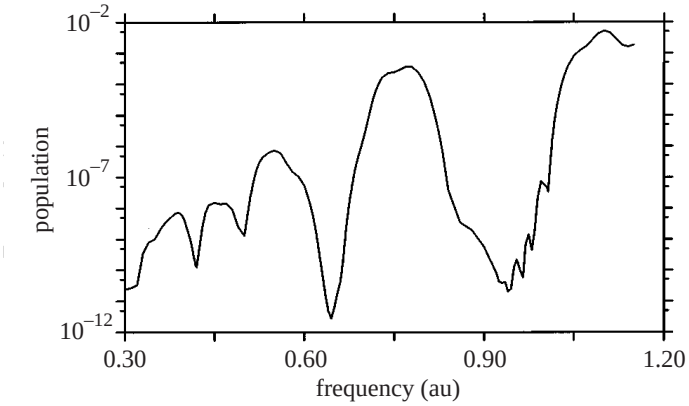

Figure 15. Populations in the doubly excited states of helium after passage of a pulse of duration 157 au and pulse energy 0.5 au.

play, and the G_{Ll_1} are two-electron angular factors for the total angular momentum L and the zero z-component of this. For each (L, l_1), several sets of exponents (α_i, β_i) were used. The $c_i^{Ll_1}(\theta, t)$ are expansion coefficients obtained from instant to instant by propagating the solution Ψ_θ of the rotated TDSE. They are complex, since the basis functions in equation (3.24) are entirely real. Moreover, they entirely contain the dependence of Ψ_θ on θ.

Calculations have been carried out exclusively in the velocity gauge and in initial calculations reported by Scrinzi & Piraux (1997), an average of 300 expansion functions were retained for each L going from 0 to $L_{\max} = 7$. Excellent values were obtained for both singly excited and doubly excited states of field-free He using these expansion functions.

In the interaction of the laser with the atom, the investigation of two-electron processes is particularly interesting, and these occur even at moderate intensities. Figure 15 depicts the total population in all doubly excited states (that can be unambiguously represented by the field-free basis) after passage of $\sin^2$ character, 3.8 fs laser pulses, of frequency ranging between 0.30 and 1.20 au (i.e. wavelengths ranging between 152 and 40 nm). These pulses were all chosen to have the same integrated pulse energy of 0.5 au. A clear resonance structure is discernible and due to the short duration of the pulse, various resonances overlap. The five broad peaks correspond roughly to two-, three-, four-, five- and six-photon transitions to the doubly excited states with even and odd angular momenta alternately, as one progresses downwards to lower photon frequencies.

In this method, the advantage of being able to work with L^2 basis functions is in many cases outweighed by the difficulty, in practice, of back-rotating the wave function Ψ_θ to that approximating the solution of the TDSE with the unrotated Hamiltonian, i.e. the solution to the true physical problem. This has not yet been attempted, but will be necessary if this method is to yield insight on wave packet ionization dynamics or knowledge of quantities, such as partial one-electron or two-electron ionization yields, for which the character of the true wave function must be known.

(v) *An R-matrix time-dependent method*

The objective of this new theory is to enable the TDSE for an arbitrary many-electron atom in an intense laser field to be solved directly using the R-matrix method. This work is complementary to the RMF work mentioned above, in that it will enable higher laser field intensities (greater than 1.0×10^{15} W cm^{-2}, where RMF calculations for many-electron atoms become computationally very demanding due to the large number of Floquet blocks that must be included to obtain convergence) and shorter laser pulses (less than 50 fs) to be studied. It will, like the RMF work, be able to take advantage of existing techniques and computer programs that have been developed over many years to treat a wide range of atomic processes using the R-matrix method (Burke & Berrington 1993).

Starting from the velocity-gauge TDSE defined by equation (2.9), the Hamiltonian, H_{N+1}, can be written as

$$H_{N+1} = -\tfrac{1}{2}\boldsymbol{\nabla}^2_{N+1} + H_N + V(\boldsymbol{X}_N, \boldsymbol{x}_{N+1}), \tag{3.25}$$

where H_N is the N-electron Hamiltonian for the residual atomic target, and

$$V(\boldsymbol{X}_N, \boldsymbol{x}_{N+1})$$

is the interaction potential between the ejected electron and the target.

$\Psi(\boldsymbol{X}_{N+1}, t)$ is now expanded as follows

$$\Psi(\boldsymbol{X}_{N+1}, t) = \mathcal{A}\sum_{i=1}^{n} \bar{\phi}_i(\boldsymbol{X}_N; \hat{\boldsymbol{r}}_{N+1}\sigma_{N+1}) r_{N+1}^{-1}\psi_i(r_{N+1}, t), \tag{3.26}$$

where $\mathcal{A}$ is the usual antisymmetrization operator, the $\bar{\phi}_i$ are channel functions formed by coupling the residual target states and, possibly, pseudo-states ϕ_i with the angular and spin eigenfunctions of the ejected electron, and the ψ_i are the time-dependent reduced functions describing the radial motion of the ejected electron in the ith channel. Substituting equation (3.26) into equation (2.9), projecting onto the channel functions $\bar{\phi}_i$, and using the equation

$$\langle \phi_i(\boldsymbol{X}_N) \mid H_N \mid \phi_j(\boldsymbol{X}_N)\rangle = w_i\delta_{ij}$$

satisfied by the ϕ_i, where w_i are the target energies, yields the following coupled partial integro-differential equations

$$\left[-\frac{1}{2}\left(\frac{\partial^2}{\partial r^2} - \frac{l_i(l_i+1)}{r^2}\right) + w_i\right]\psi_i(r,t) + \sum_{j=1}^{n}\left(P_{ij}(t)\frac{\partial}{\partial r} + W_{ij}(r,t)\right)\psi_j(r,t) = \mathrm{i}\frac{\partial}{\partial t}\psi_i(r,t), \quad i = 1,\ldots,n. \tag{3.27}$$

In this equation, the first derivative coupling term, $P_{ij}(t)\partial/\partial r$, arises from the $(1/c)\boldsymbol{A}(t)\cdot\boldsymbol{P}_{N+1}$ term in equation (2.9), where the matrix $\boldsymbol{P}(t)$ with elements $P_{ij}(t)$ is anti-Hermitian, and the kernel W_{ij} is the sum of three terms, W_{D}, the direct electron–electron and electron–nucleus interaction, W_{E}, the non-local exchange electron–electron interaction, and W_{L}, the remaining terms arising from the vector potential $\boldsymbol{A}(t)$ describing the laser field in equation (2.9).

Equation (3.27) can be conveniently written in matrix form,

$$\boldsymbol{H}(t)\boldsymbol{\psi}(r,t) = \mathrm{i}\frac{\partial}{\partial t}\boldsymbol{\psi}(r,t), \tag{3.28}$$

and a discrete mesh in time introduced

$$t_m = m\Delta t, \quad m = 0, 1, 2, \ldots, \tag{3.29}$$

in terms of a basic time-interval Δt. Employing the unitary Cayley form for the time evolution operator $\exp[-\mathrm{i}\Delta t \boldsymbol{H}]$, equation (3.28) becomes

$$\boldsymbol{\psi}(r, t_{m+1}) = \left[\frac{\boldsymbol{I} - (1/2)\mathrm{i}\Delta t \boldsymbol{H}(t_{m+(1/2)})}{\boldsymbol{I} + (1/2)\mathrm{i}\Delta t \boldsymbol{H}(t_{m+(1/2)})}\right]\boldsymbol{\psi}(r, t_m) + O(\Delta t^3), \tag{3.30}$$

which can be rewritten as

$$(\boldsymbol{H}^{m+(1/2)} - E\boldsymbol{I})\boldsymbol{\psi}^{m+1}(r) = \boldsymbol{\phi}^m(r), \quad m = 0, 1, 2, \ldots, \tag{3.31}$$

where the inhomogeneous term $\boldsymbol{\phi}^m(r)$ is given by

$$\boldsymbol{\phi}^m(r) = -(\boldsymbol{H}^{m+(1/2)} + E\boldsymbol{I})\psi^m(r). \tag{3.32}$$

Also in equation (3.31)

$$\boldsymbol{\psi}^m(r) = \boldsymbol{\psi}(r, t_m), \quad \boldsymbol{H}^{m+(1/2)} = \boldsymbol{H}(t_{m+(1/2)}) \quad \text{and} \quad E = 2\mathrm{i}(\Delta t)^{-1}. \tag{3.33}$$

In order to solve the inhomogeneous equation (3.31), the region of interest is divided into p sub-regions and an R-matrix propagator approach is followed along the lines set out by Baluja *et al.* (1982). For further details, Burke & Burke (1997) should be consulted. This paper also reports results for a model problem indicating that the procedure is stable.

4. Conclusions

In this article we have presented an overview of both recent and current theoretical investigations in the subject. The R-matrix Floquet method is appropriate for calculating the response of multielectron atoms to long-pulse intense laser radiation. For short pulses, where time-dependent approaches are essential, many of the methods discussed above can be developed further. Different methods play different roles. For instance, density functional theory will, for the foreseeable future, remain a method that best provides some measure of many-electron ionization (i.e. beyond two-electron ionization) of a multielectron atom in an intense laser field. The new time-dependent R-matrix approach, in particular, holds great promise for describing multiphoton processes in a general light multielectron atom with up to two electrons entering the continuum.

Some aspects of laser-atom physics have not yet been touched upon in theoretical work on multielectron atoms. One of the most exciting of these areas for the future must be when relativistic physics comes into play in either the motion of the atomic electrons or in the description of the laser, or indeed into both!

The preparation of this article has been supported in part by the UK Engineering and Physical Sciences Research Council. The authors much appreciate discussions with, and contributions from, their colleagues in Queen's University Belfast, namely, Phil Burke, David Glass, Jonathan Parker and Edward Smyth.

References

Baluja, K. L., Burke, P. G. & Morgan, L. A. 1982 *Comp. Phys. Commun.* **27**, 299.

Bauer, D. 1997 *Phys. Rev.* A **56**, 3028.
Becker, A. & Faisal, F. H. M. 1996 *J. Phys. Lett.* B **29**, 197.
Bloch, C. 1957 *Nucl. Phys.* **4**, 503.
Burke, P. G. & Berrington, K. A. 1993 *Atomic and molecular processes: an R-matrix approach.* Bristol and Philadelphia, PA: Institute of Physics.
Burke, P. G. & Burke, V. M. 1997 *J. Phys. Lett.* B **30**, 383.
Burke, P. G., Hibbert, A. & Robb, W. D. 1971 *Adv. At. Mol. Phys.* **10**, 11.
Burke, P. G., Franken, P. & Joachain, C. J. 1990 *Europhys. Lett.* **13**, 617.
Burke, P. G., Franken, P. & Joachain, C. J. 1991 *J. Phys.* B **24**, 761.
Buttle, P. J. A. 1967 *Phys. Rev.* **160**, 719.
Dörr, M., Terao-Dunseath, M., Purvis, J., Noble, C. J., Burke, P. G. & Joachain, C. J. 1992 *J. Phys.* B **25**, 2809.
Dundas, D., Taylor, K. T., Parker, J. S. & Smyth, E. S. 1999*a* *J. Phys.* B. (In the press.)
Dundas, D., Parker, J. S. & Taylor, K. T. 1999*b*. (In preparation.)
Eberly, J. H. 1990 *Phys. Rev.* A **42**, 5750.
Eberly, J. H. & Grobe, R. 1994 In *Super-intense laser atom physics* (ed. B. Piraux, A. L'Huillier & K. Rzążewski), pp. 445. New York: Plenum.
Erhard, S. & Gross, E. K. U. 1996 In *Multiphoton Processes 1996: Proc. of the 7th Int. Conf. on Multiphoton Processes* (ed. P. Lambropoulos & H. Walther), pp. 37. Bristol: Institute of Physics.
Floquet, G. 1883 *Ann. Ec. Norm.* **13**(2), 47.
Gębarowski, R., Burke, P. G. & Taylor, K. T. 1997 *J. Phys.* B **30**, 2505.
Glass, D. H., Burke, P. G., Van der Hart, H. W. & Noble, C. J. 1997 *J. Phys.* B **30**, 1697.
Glass, D. H., Burke, P. G., Noble, C. J. & Wöste, G. B. 1998 *J. Phys. Lett.* B **31**, 667.
Grobe, R. & Eberly, J. H. 1992 *Phys. Rev. Lett.* **68**, 2905.
Grobe, R. & Eberly, J. H. 1993*a* *Phys. Rev.* A **47**, R1605.
Grobe, R. & Eberly, J. H. 1993*b* *Phys. Rev.* A **48**, 623.
Gross, E. K. U., Dobson, J. F. & Petersilka, M. 1996 In *Density functional theory II* (ed. R. F. Nalewajski), pp. 81. Berlin: Springer.
Haan, S. L., Grobe, R. & Eberly, J. H. 1994 *Phys. Rev.* A **50**, 378.
Hermann, M. R. & Skillman, S. 1963. *Atomic structure calculations.* Englewood Cliffs, NJ: Prentice-Hall.
Hohenberg, P. & Kohn, W. 1964 *Phys. Rev.* **136**, B864.
Horbatsch, M. 1994 *Z. Phys.* D **30**, 31.
Horbatsch, M., Lüdde, H. J. & Dreizler, R. M. 1992 *J. Phys.* B **25**, 3315.
Javanainen, J., Eberly, J. H. & Su, Q. 1988 *Phys. Rev.* A **38**, 3430.
Joachain, C. J. 1996 In *Multiphoton Processes 1996: Proc. of the 7th Int. Conf. on Multiphoton Processes* (ed. P. Lambropoulos & H. Walther), pp. 46. Bristol: Institute of Physics.
Kohn, W. & Sham, L. J. 1965 *Phys. Rev.* A **140**, 1133.
Krause, J. L., Shafer, K. J. & Kulander, K. C. 1992 *Phys. Rev.* A **45**, 4998.
Krieger, J. B., Li, Y. & Iafrate, G. J. 1990 *Phys. Lett.* A **146**, 256.
Kulander, K. C. 1987*a* *Phys. Rev.* A **35**, 445.
Kulander, K. C. 1987*b* *Phys. Rev.* A **36**, 2726.
Kulander, K. C. 1988 *Phys. Rev.* A **38**, 778.
Kulander, K. C., Shafer, K. J. & Krause, J. L. 1992 In *Atoms in intense laser fields* (ed. M. Gavrila), pp. 247. New York: Academic.
Kylstra, N. J., van der Hart, H. W., Burke, P. G. & Joachain, C. J. 1998 *J. Phys.* B **31**, 3089.
Lambropoulos, P. & Tang, X. 1994 In *Super-intense laser atom physics* (ed. B. Piraux, A. L'Huillier & K. Rzążewski), pp. 403. New York: Plenum.

Lappas, D. G. & van Leeuwen, R. 1998 *J. Phys. Lett.* B **31**, 249.
Lappas, D. G., Sanpera, A., Watson, J. B., Burnett, K., Knight, P. L., Grobe, R. & Eberly, J. H. 1996 *J. Phys. Lett.* B **29**, 619.
Li, X. F., L'Huillier, A., Ferray, M., Lompré, L. A. & Mainfray, G. 1989 *Phys. Rev.* A **39**, 5751.
Parker, J., Taylor, K. T., Clark, C. W. & Blodgett-Ford, S. 1996 *J. Phys. Lett.* B **29**, 33.
Parker, J., Smyth, E. & Taylor, K. T. 1998 *J. Phys. Lett.* B **31**, 571.
Parker, J., Smyth, E. & Taylor, K. T. 1999. (In preparation.)
Pindzola, M. S., Griffin, D. C. & Bottcher, C. 1991 *Phys. Rev. Lett.* **66**, 2305.
Pindzola, M. S., Garvas, P. & Gorczyca, T. W. 1995 *Phys. Rev.* A **51**, 3999.
Potvliege, R. M. & Shakeshaft, R. 1988 *Phys. Rev.* A **38**, 4597.
Preston, S. G. (and 10 others) 1996 *Phys. Rev.* A **53**, R31.
Runge, E. & Gross, E. K. U. 1984 *Phys. Rev. Lett.* **52**, 997.
Sanpera, A., Jönsson, P., Watson, J. B. & Burnett, K. 1995 *Phys. Rev.* A **51**, 3148.
Scrinzi, A. & Piraux, B. 1997 *Phys. Rev.* A **56**, R13.
Sharp, R. T. & Horton, G. K. 1953 *Phys. Rev.* **90**, 317.
Smyth, E., Parker, J. & Taylor, K. T. 1998 *Comp. Phys. Commun.* **114**, 1.
Talman, J. D. & Shadwick, W. F. 1976 *Phys. Rev.* A **14**, 36.
Tang, X., Rudolph, H. & Lambropoulos, P. 1990 *Phys. Rev. Lett.* **65**, 3269.
Tang, X., Rudolph, H. & Lambropoulos, P. 1991 *Phys. Rev.* A **44**, R6994.
Taylor, K. T., Parker, J., Dundas, D., Smyth, E. & Vivirito, S. 1996 In *Multiphoton Processes 1996: Proc. of the 7th Int. Conf. on Multiphoton Processes* (ed. P. Lambropoulos & H. Walther), pp. 56. Bristol: Institute of Physics.
Taylor, K. T., Parker, J., Dundas, D., Smyth, E. & Vivirito, S. 1997 In *Proc. of PECAM II* (ed. P. G. Burke & C. J. Joachain), pp. 223. New York: Plenum.
Ullrich, C. A., Gossmann, U. J. & Gross, E. K. U. 1995*a* *Phys. Rev. Lett.* **74**, 872.
Ullrich, C. A., Gossmann, U. J. & Gross, E. K. U. 1995*b* *Ber. BunsenGes. Phys. Chem.* **99**, 488.
Walker, B., Mevel, E., Yang, B., Breger, P., Chambaret, J. P., Antonetti, A., DiMauro, L. F. & Agostini, P. 1994 *Phys. Rev.* A **48**, R894.
Watson, J. B., Sanpera, A., Lappas, D. G., Knight, P. L. & Burnett, K. 1997 *Phys. Rev. Lett.* **78**, 1884.
Wigner, E. P. 1946 *Phys. Rev.* **70**, 15.
Zhang, J. & Lambropoulos, P. 1995 *J. Phys. Lett.* B **28**, 101.

PHILOSOPHICAL TRANSACTIONS OF THE ROYAL SOCIETY A MATHEMATICAL, PHYSICAL & ENGINEERING SCIENCES